Hydrodynamic Feedback on Bubble Breakup at a T-junction Within an Asymmetric Loop

Taotao Fu
State Key Laboratory of Chemical Engineering, School of Chemical Engineering and Technology, Tianjin University, Tianjin 300072, China

Laboratory of Reactions and Process Engineering, University of Lorraine, CNRS, 1, rue Grandville, BP 20451, Nancy Cedex 54001, France

Youguang Ma
State Key Laboratory of Chemical Engineering, School of Chemical Engineering and Technology, Tianjin University, Tianjin 300072, China

Huai Z. Li
Laboratory of Reactions and Process Engineering, University of Lorraine, CNRS, 1, rue Grandville, BP 20451, Nancy Cedex 54001, France

DOI 10.1002/aic.14377
Published online February 5, 2014 in Wiley Online Library (wileyonlinelibrary.com)

Bubble breakup at a microfluidic T-junction by taking into consideration the hydrodynamic feedback at the downstream channels is presented. Experiments are conducted in square microchannels with 400 μm in width. The splitting ratio of the bubble size in the bifurcations varies nonmonotonically with the flow rate ratio of gas/liquid phases, and it is also affected by the liquid viscosity. A critical size of the mother bubble determines the variation trend of the splitting ratio of bubble size with flow rates of both phases and the liquid viscosity, which is related to the different breakup mechanisms for long and short bubbles at the junction and the different additional resistances induced by long and short bubbles in downstream channels. A theoretical model is proposed to predict the tailoring size of bubbles at the T-junction by taking into account of the additional resistance in the presence of bubbles in downstream channels. © 2014 American Institute of Chemical Engineers *AIChE J*, 60: 1920–1929, 2014
Keywords: bubble, multiphase flow, microfluidics, hydrodynamic feedback

Introduction

Microfluidic multiphase flow is an emerging technology with characteristics of controllability, smart, and small, and displays potential advantages in materials synthesis, emulsions, drug encapsulation, crystallization, chemical mixing, and reaction.[1–5] Bubbles and droplets are always encountered in these applications and they are generated, transported, and manipulated using several basic microfluidic configurations, such as T- and Y-junctions, flow-focusing and coflowing junctions for the generation,[6–11] straight and zigzag channels for the transportation,[12,13] parallel channels, and multistages bifurcations for the manipulation.[13–18]

T-junction is one of the most basic elements in microdevices for the manipulation of bubbles and droplets.[19–22] The bubble and droplet behavior is highly nonlinear at the junction owing to the hydrodynamic collective feedback or hydrodynamic memory—the interplay of coherent resistance of the channels and the additional resistance arisen by the bubbles and droplets, and even the collision, breakup, repartition of the bubbles and droplets.[23–27] For example, bubbles and droplets can breakup or do not breakup at the T-junction, depending mainly on their sizes and the capillary number.[19,28–30] For the nonbreaking case, repartition and filtering regimes are observed, owing to the flow rates in the arms of the junctions.[21,25,31–33] Jeanneret et al.[34] recently focused on the transport of particles in one-dimensional loop networks and showed that the dynamics is asymptotically invariant upon time-reversal symmetry. Sessoms et al.[25] introduced a model to understand the collective time-delayed feedback mechanism for the binary path selection of droplets arriving at a T-junction, which are related to the retention times of the droplets in the loop, yielding the complex dynamics. Parthiban and Khan[35] found a filter regime for bubbles flowing through a symmetric junction, as the resistance to the flow decreases with an increase in the number of bubbles in the microchannel. For the breaking case, symmetric and asymmetric breakup of bubbles and droplets are observed for both symmetric and asymmetric T-junctions, relating to the flow rates in each arms of the junctions and the local pressure at the junction.[19,28,36–43] Song et al.[26] investigated recently the local interactions and the global organization of a two-phase flow in a branching tree and found that the evolution of a plug at the junctions depends on the interplay between a

Correspondence concerning this article should be addressed to Y. Ma at ygma@tju.edu.cn, and H.Z. Li at Huai-Zhi.Li@univ-lorraine.fr.

dynamically determined pressure and a geometrically controlled threshold value, resulting in nonlinear characteristics. Hoang et al.[22] performed three-dimensional numerical simulations to study the droplet breakup in a T-junction and observed two distinct breakup stages: a quasisteady droplet deformation driven by the applied flow and a surface tension-driven rapid pinching which is independent of the applied flow. They also found two different critical conditions: one determines whether the droplet breaks or not, and other sets when the rapid pinching starts.

The flow rate in each arms of the T-junction is controlled by the resistance through channels, comprising the coherent resistance of the channel and the resistance induced by the bubbles and droplets, and also influenced by the collision of bubbles and droplets at the junction.[27,35,44] Bedram and Moosavi[39] performed numerical investigation on droplet breakup in an asymmetric T-junction, and indicated that smaller droplets can be generated by increasing the capillary number. When the T-junction is used to tailor droplets into smaller ones, small deviations are observed for the tailoring sizes of droplets between the experimental data and the theoretical values estimated based on the assumption that the breaking size of droplets is determined by the coherent resistance in the channels.[19,37,42] Link et al.[19] pioneered to use a T-junction to tailor droplets passively and found that the size of daughter droplets could be controlled by adjusting the length of arms of the T-junction. A slight discrepancy was observed for the tailoring size of droplets between the coherent resistance and the experiments owing to the presence of a large number of droplets in channels. Yamada et al.[37] manipulated droplet division by using hydrodynamic control of the bifurcating microchannels and found that the theoretical estimation stemming from the inherent resistance of the microchannel should be improved by taking into consideration the resistance induced by the effects of pressure at the interface between two phases due to the presence of droplets. Samie et al.[42] conducted theoretical and experimental investigation on the breakup of droplets in an asymmetric T-junction with branches of identical lengths and different cross-sections to produce unequal-sized droplets. They found that the volume ratio for the generated droplets in each arm of the junction is only a function of the geometry. Furthermore, they also found small deviation between the experimental data and theoretical prediction, which is due to the hydrodynamic resistance induced by the presence of the droplets in microchannels. These studies suggest that the resistance induced by the dispersed phase in the channels should be taken into consideration for the tailoring of bubbles and droplets by using the T-junction.

Although several efforts have been devoted to the breakup of droplets and bubbles at T-junctions, the study on hydrodynamic feedback on the breakup of bubbles is still missing up to now. This work aims at studying bubble breakup at a microfluidic T-junction within an asymmetric loop, by taking into account the hydrodynamic collective feedback in downstream microchannels.

Experimental Setup

The experimental setup is sketched in Figure 1. The microfluidic device includes the bubble formation section and the bubble breakup section in a loop, as shown in Figure 1a. In a first T-junction of the loop, the microchannel divides into two asymmetric parts of the same section but different

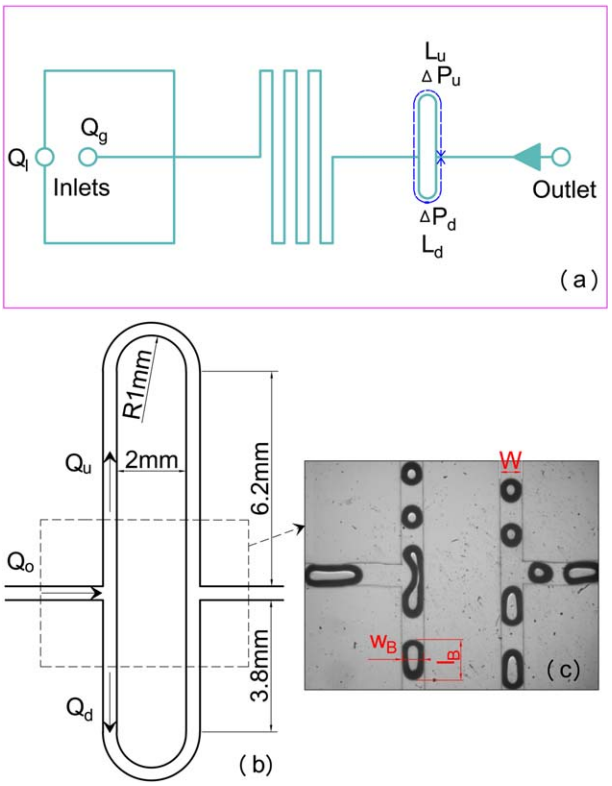

Figure 1. (a) The microfluidic device used in the experiments.

Bubbles are formed in the cross junction and move toward a snake-like channel and then to a loop with the length of the upper arm L_u and of the lower arm L_d. (b) The microfluidic loop used in the experiments. The flow diverges at the first T-junction and recombines at the second T-junction. (c) A picture captured by a high-speed camera. Bubbles can breakup at the first T-junction bifurcation. [Color figure can be viewed in the online issue, which is available at wileyonlinelibrary.com.]

length, and then the two channels merge at a second T-junction to form a single channel again. The lengths of the arms are shown in Figures 1a, b. Bubbles are formed in a microfluidic flow-focusing junction (the left hand diagram of Figure 1a), and move toward the loop (the right hand diagram of 1a). Bubbles can break at the first T-junction and exit the second one into the single channel (Figure 1c). The microfluidic device is fabricated in a polymethyl methacrylate (PMMA) plate ($70 \times 35 \times 10$ mm^3) by precision milling and sealed by another thin PMMA plate. The cross-section is 400-μm wide and 400-μm high. Gas is fed by a N_2 cylinder. The gas flow rate is controlled by a high precision micrometering valve (Sagana Instrumentation, Luxembourg), and calibrated by a soap bubble flowmeter at the inlet of the microdevice. Liquid is delivered from a 60-mL syringe by a syringe pump (Harvard Apparatus, PHD 22/2000). All of our experiments are conducted at room temperature and atmospheric pressure.

The microfluidic device is placed under an inverted microscope (Leica, Germany), which is equipped with a high-speed camera CamRecord600 (Optronis GMBH, Germany, up to 100,000 frames per second). In this work, the frame rates are between 200 and 1000 fps. The images are processed by a Matlab program to obtain the quantitative features of bubbles. A micro-Particle Image Velocimetry system (micro-PIV)

Table 1. Properties of the Experimental Gas–liquid Systems Used in this Work

Liquid Phase	Surface Tension, σ (mN m^{-1})	Viscosity, μ (mPa s)	Density, ρ (kg m^{-3})
0.5% SDS/water	33	0.92	1000
0.5% SDS/25% glycerol	31.5	2.32	1060
0.5% SDS/50% glycerol	31.5	6.53	1130
0.5% SDS/62% glycerol	31.5	10.18	1160

(Dantec Dynamics, Denmark) is used to obtain velocity fields in the continuous phase around the bubbles at the T-junction as described in the previous work.[28]

Three different glycerol (Prolabo, France) concentrations of 25, 50, and 62 wt % are mixed with deionized water to vary the viscosity of the liquid phase. Sodium dodecyl sulfate (SDS) (Amresco) (0.5 wt %) is used as surfactant in the aqueous phase to modify the surface tension and to stabilize the bubbles against coalescence. A Rheometric Fluid Spectrometer RFS II (Rheometric Scientific) is used to characterize the viscosity of the liquids. The surface tension is measured by a tensiometer based on the pendant drop technique on a Tracker apparatus (I.T. Concept, France). The contact angle of the liquid on a flat PMMA surface is about 60°. The various properties of the experimental systems are gathered in Table 1.

The volume of the bubbles V is calculated by the following equations

$$V=\begin{cases} \pi l_B w_B((l_B+w_B)/2)/6 & l_B < W, w_B < W \\ 4\pi(w_B/2)^3/3+0.9w_B^2(l_B-w_B) & l_B > W \end{cases} \quad (1)$$

When the bubbles are smaller than the channel width, they are assumed as ellipsoid and their volumes can be obtained using the expression of the first line in Eq. 1. When the bubbles are larger than the channel width, they are named as slug bubbles and have two semispheroid ends for the rears and tips of the bubbles and nearly cylindrical bodies occupying about 90% of the channel with the same length as the cylindrical bodies and the volume of the bubbles can be calculated using the expression of the second line in Eq. 1.[45] The accuracy of Eq. 1 was checked by comparing the computed volume of the mother bubble with that of the daughter bubbles, and the relative error is below 5%. The experimental conditions are as follows: $0.12 \le Q_g/Q_l \le 3.34$, $0.0016 \le Ca \le 0.10$, $0.3 \le Re \le 310$, where l_B is the length of the daughter bubbles, w_B the width of the bubble, W the width of the channel. Q_g and Q_l are the volumetric flow rates of the gas and liquid phases, respectively. Ca ($Ca=\mu u/\sigma$) is the capillary number, and μ the liquid viscosity, u ($u=(Q_g+Q_l)/W^2$) the superficial velocity of the gas–liquid flow, σ the surface tension between the liquid phase and N_2. Re ($Re=\rho uW/\mu$) is the Reynolds number, and ρ the density of the liquid phase.

Results and Discussion

Tailoring size of bubbles in the two branches of the T-junction

The size ratio of bubbles in the two branches of the T-junction V_u/V_d is shown in Figures 2 and 3, where V_u and V_d are the volume of bubbles at the upper arm and lower arm, respectively. We found that (1) the ratio of the size of daughter bubbles V_u/V_d is not consistent with the theoretical value 0.74 calculated by assuming that the volume of the daughter bubbles is determined by the flow rate in the channel, which is inversely proportional to the coherent resistance of the channel: $V_u/V_d \propto Q_u/Q_d \propto R_{od}/R_{ou} \propto L_d/L_u$,[46] where Q_u and Q_d are the volumetric flow rate of gas–liquid

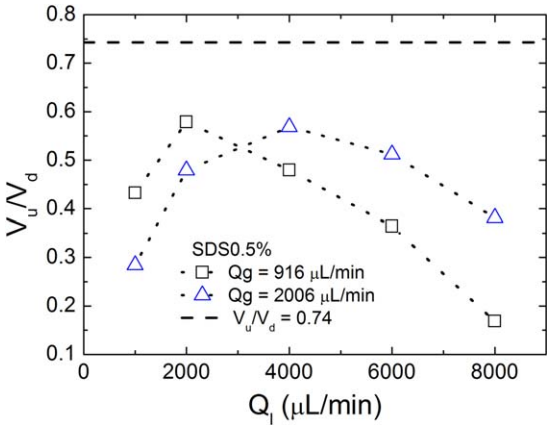

Figure 2. Effects of gas and liquid flow rates on the splitting ratio of bubble size in the two arms.

[Color figure can be viewed in the online issue, which is available at wileyonlinelibrary.com.]

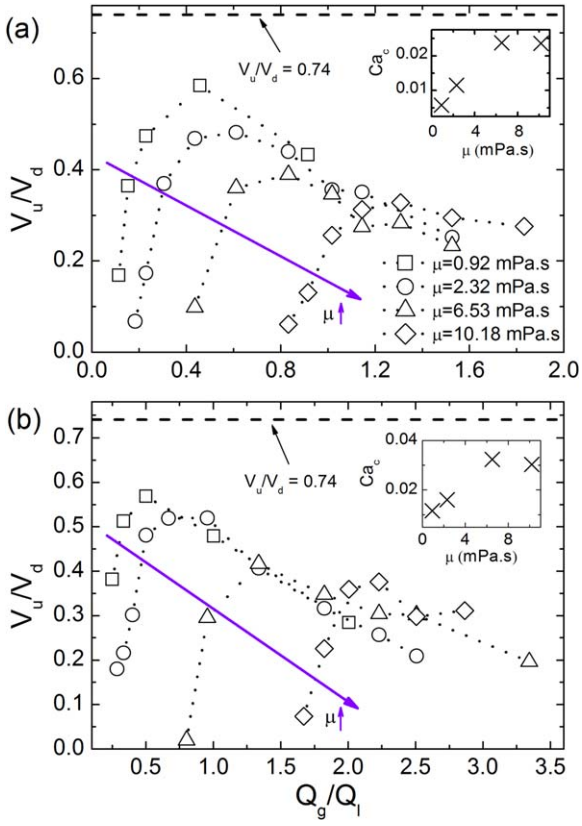

Figure 3. Effects of the flow rate ratio of gas/liquid phases and the liquid viscosity on the splitting ratio of bubble size in the two arms.

(a) $Q_g = 916$ μL/min, (b) $Q_g = 2006$ μL/min. [Color figure can be viewed in the online issue, which is available at wileyonlinelibrary.com.]

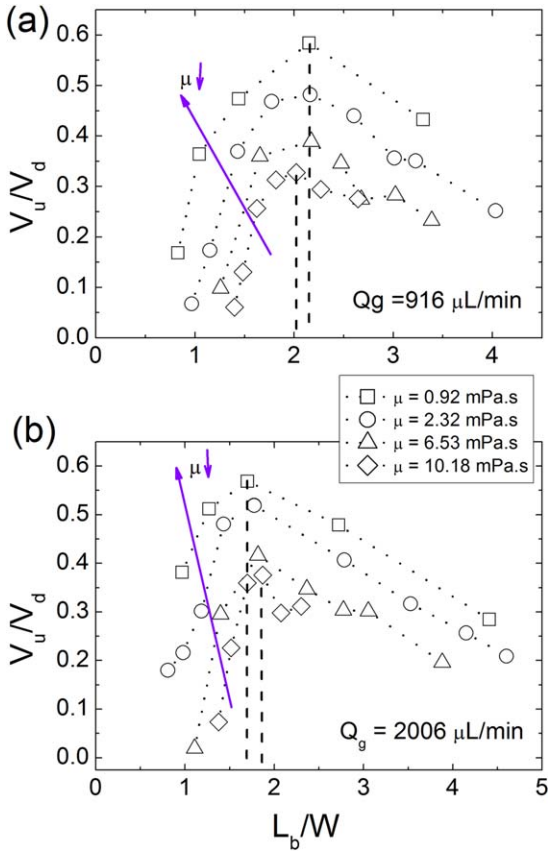

Figure 4. Effects of the size of the mother bubble on the splitting ratio of bubble size in the two arms.

The vertical lines represent the critical bubble length $(L_b/W)_c$ for each set of data for various liquid phases. (a) $Q_g = 916$ μL/min, (b) $Q_g = 2006$ μL/min. [Color figure can be viewed in the online issue, which is available at wileyonlinelibrary.com.]

two-phase in the upper and lower arms of the T-junction, respectively, R_{ou} and R_{od} are the coherent resistance in the upper and lower arms of the T-junction, respectively, L_u and L_d the length of the upper and lower arms of the T-junction, respectively; (2) V_u/V_d is affected by the gas and liquid flow rates and the liquid viscosity. For a given gas flow rate, V_u/V_d first increases before decreasing with the increase of the liquid flow rate. The crossover point of the liquid flow rate increases with the increase of the gas flow rate as shown in Figure 2. The crossover point of V_u/V_d decreases, whereas that of the Q_g/Q_l increases with the increase of the liquid viscosity. Although the crossover point of the capillary number increases with the liquid viscosity and levels off when the liquid viscosity is over 6.53 mPa s. These intriguing phenomena motivate us to find out answers to following questions: what determines the size of the daughter bubbles, why there is a turning point for the $V_u/V_d \sim Q_g/Q_l$ curve, and why it is affected by the liquid viscosity?

Effects on the resistance in the microchannel

The resistance in the channel could be modified by the presence of bubbles, and the supplementary resistance induced by bubbles is determined by both of the size and number of bubbles within the channel.[19,21,47,48] Therefore, the tailoring size of the daughter bubbles not only relies on the coherent resistance in the channel but also on the additional resistance due to the feedback of bubbles in downstream channels. Link et al.[19] also observed the discrepancy between the theoretical value calculated using the coherent resistance in the channel and the experimental data for the tailoring size of droplets in an asymmetric T-junction, and gave an tentative explanation that the presence of droplets in the long channel could change the resistance in the channel. The dependence of V_u/V_d on Q_g/Q_l and the liquid viscosity could be explained by the fact that both of the size and number of bubbles within the channels are determined by the Q_g/Q_l and the liquid viscosity as revealed for bubbles generated in a microfluidic flow-focusing device.[49] Therefore, the excess resistance due to the presence of bubbles within the channel depends on Q_g/Q_l and the liquid viscosity.

Breakup mechanism at the T-junction

The turning point in the relation $V_u/V_d \sim Q_g/Q_l$ can be attributed to the fact that the additional resistance induced by the bubbles rely on their sizes and number in channels[19,21,47,48] according to the gas and liquid flow rates and the liquid viscosity.[49] When long enough, bubbles are bounded by the channel walls, and the pressure drop across bubbles falls into the Bretherton regime and can be related to the capillary number Ca.[50] For bubbles smaller than the channel width, the resulting additional resistance could be expressed by a representative length proposed by Engl

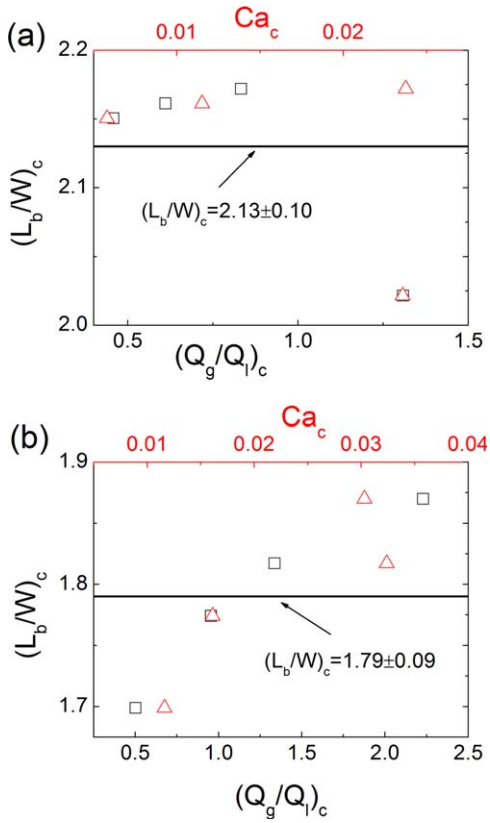

Figure 5. Critical effects of the gas/liquid flow rate ratio and capillary number on the size of the mother bubble.

(a) $Q_g = 916$ μL/min, (b) $Q_g = 2006$ μL/min. (□) $(L_b/W)_c \sim (Q_g/Q_l)_c$, (Δ)$(L_b/W)_c \sim Ca_c$. [Color figure can be viewed in the online issue, which is available at wileyonlinelibrary.com.]

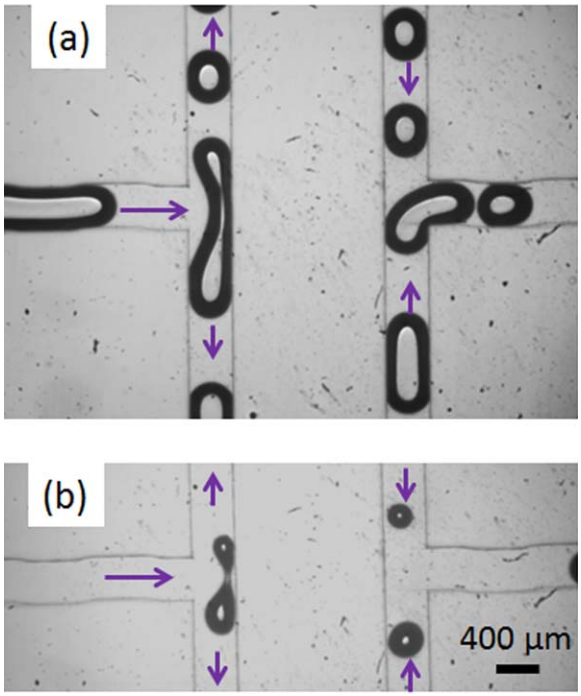

Figure 6. Breakup of long and short bubbles.

Liquid phase: 0.5% SDS aqueous solution. (a) Long bubble, $L_b/W = 3.30$; (b) Short bubble, $L_b/W = 1.04$. [Color figure can be viewed in the online issue, which is available at wileyonlinelibrary.com.]

et al.,[21] which is a function of the viscosity ratio of the dispersed phase to the continuous one and of the confinement factor as expressed by the bubble diameter normalized by the channel width l_B/W.

The dependence of V_u/V_d on the relative length of bubbles L_b/W for various liquid viscosities and gas flow rates is plotted in Figure 4, where L_b is the length of the mother bubble and is increased by decreasing the liquid flow rate Q_l at a given gas flow rate.[49] At a fixed L_b/W, V_u/V_d increases with the increase of the liquid viscosity. V_u/V_d increases with L_b/W until to a maximum value $(V_u/V_d)_c$ before decreasing. Whatever the liquid viscosity is, a critical bubble length $(L_b/W)_c$ does exist and determines the turning of V_u/V_d as shown in Figure 4. The critical bubble length $(L_b/W)_c$ remains relatively constant, which seems to be correlated to the gas flow rate as shown in Figures 4 and 5. Furthermore, the crossover of the V_u/V_d is determined by the critical bubble length $(L_b/W)_c$ rather than the critical flow rate ratio of gas and liquid phases $(Q_g/Q_l)_c$ and the critical capillary number Ca_c, as shown in Figure 5. For $Q_g = 916$ μL/min, $(L_b/W)_c = 2.13 \pm 0.10$, $Ca_c \in [0.0058, 0.024]$, $(Q_g/Q_l)_c \in [0.46, 1.31]$ and for $Q_g = 2006$ μL/min, $(L_b/W)_c = 1.79 \pm 0.09$, $Ca_c \in [0.012, 0.033]$, $(Q_g/Q_l)_c \in [0.50, 2.23]$. This reveals that the bubble length is determined by the gas and liquid flow rates and the liquid viscosity, the latter one could be expressed in a dimensionless form Ca_c.[49] The critical bubble length can be understood by the fact that the additional resistance in the microchannel due to the presence of bubbles depends on the bubble size as stated before,[21,50] and the breakup of bubbles at a T-junction is either driven by pressure decrement in a narrow gap between the bubble and the channel wall for partly or totally obstructed long bubbles[28,30,51] or driven by the Rayleigh–Plateau instability for nonobstructed short bubbles.[19,28] The dynamical breakup of bubbles is affected by the local pressure drop between the rear and tips of the breaking bubble in the three arms of the T-junction.[26,30,36,52] The typical pictures for the breakup of long and short bubbles at the T-junction with bubbles flowing through the downstream channels are shown in Figure 6. It is interesting

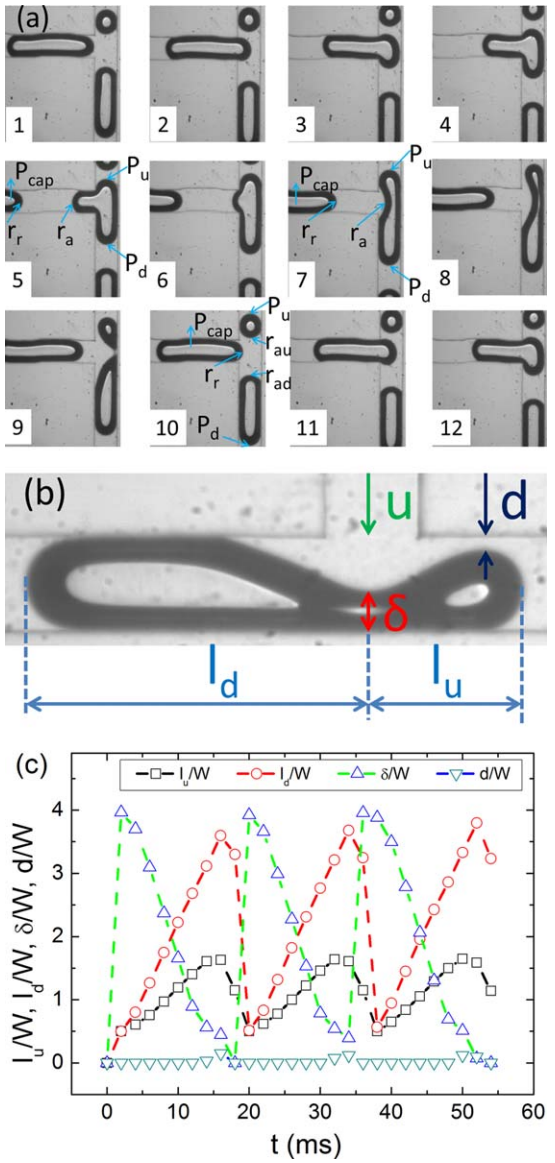

Figure 7. Bubble breakup dynamics at the T-junction.

(a) Evolution of bubble breakup at the T-junction. Time interval between the successive pictures is 2 ms. P_{cap} is the pressure in the bubble before arriving at the junction. P_u and P_d are the pressure at the tips of the invading bubble in the upper and lower arms of the junction, respectively. r_r and r_a are the radii of curvature of the rear and front interfaces, respectively. r_{au} and r_{ad} are the radii of curvature of the front interface in the upper and lower arms of the junction, respectively. (b) Characteristic parameters for the bubble breakup. u is the superficial velocity of the gas–liquid two-phase, d the minimum distance for the gap between the bubble and the wall at the upper arm, δ the thickness of the bubble neck at the junction, l_u and l_d the length of the invading bubble at the upper and lower arms of the junction, respectively and t the time. (c) Evolution of the characteristic parameters for the bubble breakup. Liquid phase: 0.5% SDS aqueous solution with 25% glycerol, $Q_g = 916$ μL/min; $Q_l = 600$ μL/min. [Color figure can be viewed in the online issue, which is available at wileyonlinelibrary.com.]

to note that a critical length is also proposed to characterize the breakup process for droplets in microfluidic junctions of arbitrary angles[36] and to identify a permanently obstructed regime for droplet breakup at a symmetric T-junction at low capillary numbers.[29] Our study extends this notion and suggests that the idea of introducing a characteristic length to describe the breakup of bubbles and droplets in microfluidic junctions can be generalized.

To gain insights into the breakup dynamics of long bubbles at the T-junction, the evolution of the interface during the breakup is traced as shown in Figure 7. The entire process for the bubble crossing the junction could be divided into two stages: the filling stage as shown in No. 1–6 and the breaking stage in No. 7–10 in Figure 7a. In the filling stage, the invading bubble bifurcates at the T-junction, and the repartition of the bubble in each arm is determined by the resistance in each branch.[36] Therefore, the portion of the bubble in the lower channel is greater than that in the upper one, as the resistance is lower in the lower channel. After the repartition of the invading bubble in the T-junction, the pressure drop of the two nods in the loop is balanced in the two arm channels. During the breaking process, a deformed neck is formed at the junction and is thinned by the dynamic local pressure as demonstrated by Leshansky and Pismen[30] and Song et al.[26] The characteristic parameters involved in the breaking process of bubbles are illustrated in Figure 7b and the evolution for these parameters is also shown in Figure 7c. The velocities of the tips of the invading bubble keep constant before the gap is opening. And, the gaseous neck also thins at a constant velocity in the filling stage, and then decelerates in the breaking stage. The explanation can arise from by the fact that the pressure variation is position-dependent owing to the interface deformations[26]. And, the capillary pressure drop P_{cap} exists at a given position, which may resist to the driving force[26]: $P_{cap}=\sigma/r_r-\sigma/r_a$. In the filling stage, the interface of the rear of the invading bubble remains unchanged, whereas in the breaking stage, the interface of the rear of the invading bubble is heavily deformed. Therefore, the thinning rate of the bubble is smaller in the breaking stage. Furthermore, as the invading of the bubble at the T-junction is determined by the dynamic local pressure, the pressures at the tips of the bubble P_u and P_d also play a key role for the bubble breakup and for the repartition of the daughter bubbles, which are determined by the resistance in the downstream channels in the presence of bubbles and plugs. The dynamical local velocity distributions around the breaking bubble at the T-junction obtained by the micro-PIV technique prove the aforementioned statements, as shown in Figure 8.

Theoretical prediction for the repartition of bubbles at the T-junction

Resistance of Long Bubbles in the Microchannel. The flow rate in each of the arm branches determines the volume of the daughter bubble: $V_u/V_d \propto Q_u/Q_d \propto R_d/R_u$, where R_u and R_d are the resistance in the presence of bubbles for the upper and lower arms of the T-junction, respectively. The coherent resistance in the channel R_o with a pure fluid flowing through it at a flow rate of Q could be estimated by the following expression[46]

$$\Delta P_L=\frac{12\left[1-\frac{192H}{\pi^5 W}\tanh\left(\frac{\pi W}{2H}\right)\right]^{-1}\mu LQ}{WH^3}=QR_o \tag{2}$$

where ΔP_L is the pressure drop along the channel with a length L, width W, and height H, μ is the viscosity of the fluid within the channel.

Bubbles within the channel can induce additional resistance to the flow, and the pressure drop across a single bubble within the microchannel ΔP_B can be evaluated by the proposal of Bretherton[50] for $Ca \le 10^{-2}$ and of Ratulowski and Chang[53] for $10^{-2} \le Ca \le 10^{-1}$, by assuming Bretherton's law[50] to be valid in square cross-section[52]

$$\Delta P_B=\begin{cases} 3.58\dfrac{\sigma}{r}\left(\dfrac{3\mu u}{\sigma}\right)^{2/3}, Ca \le 10^{-2} \\ 3.58\dfrac{\sigma}{r}\left(\dfrac{3\mu u}{\sigma}\right)^{2/3}-9.07\dfrac{\sigma}{r}\left(\dfrac{3\mu u}{\sigma}\right)^{0.95}, 10^{-2} \le Ca \le 10^{-1} \end{cases} \tag{3}$$

The influence of bubble size and bubble number on the resistance can be obtained by the following relationships

$$\Delta P=\Delta P_f+\Delta P_e \tag{4}$$

$$\Delta P_f=\Delta P_L(1-\phi) \tag{5}$$

$$\Delta P_e=n_B\Delta P_B \tag{6}$$

$$n_B=\frac{L}{l_B+l_S} \tag{7}$$

where ΔP_f is the pressure drop induced by the liquid in the channel, and ΔP_e is the pressure drop induced by the bubbles. $\phi(\phi=n_B l_B/L)$ is approximately the volumetric fraction occupied by bubbles with the length of l_B and number of n_B. l_S is the length of the liquid plug. The pressure drop across the upper channel ΔP_u and the lower channel ΔP_d in the loop should be in equilibrium: $\Delta P_u-\Delta P_d=0$, and the mass conservation law makes $Q_o=Q_u+Q_d=Q_g+Q_l$, and Q_o is the total flow rate of the gas–liquid two-phase flow in the microchannel.

According to the aforementioned reasoning, the resistance in a channel containing both liquids and bubbles R could be expressed as

$$R=R_o(1-\phi)+n_B R_B \tag{8}$$

$$R_o=\frac{12\left[1-\frac{192H}{\pi^5 W}\tanh\left(\frac{\pi W}{2H}\right)\right]^{-1}\mu L}{WH^3} \tag{9}$$

$$R_B=\frac{\Delta P_B}{uWH} \tag{10}$$

where R_B is the resistance induced by a single bubble. Therefore, for square microchannels

$$R=\begin{cases} 28.36\mu\left(L-n_B l_B+n_B\times 0.53\times Ca^{-1/3}\cdot W\right)/W^4 & Ca \le 10^{-2} \\ 28.36\mu\left(L-n_B l_B+n_B\times 0.53\times Ca^{-1/3}\cdot W-n_B\times 0.64\times Ca^{-0.05}\cdot W\right)/W^4 & 10^{-2} \le Ca \le 10^{-1} \end{cases} \tag{11}$$

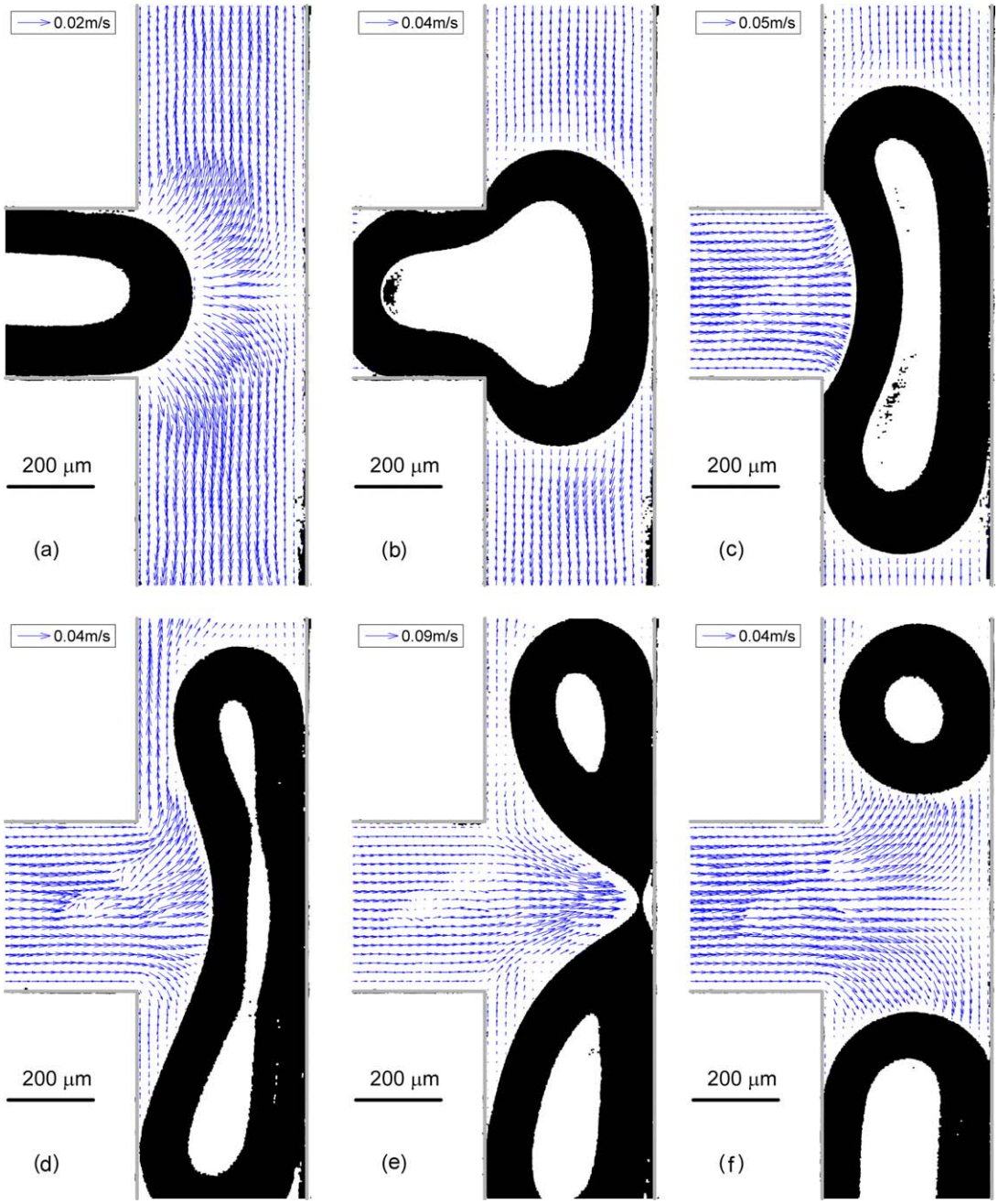

Figure 8. Velocity fields in the liquid phase around the breaking bubble at the junction obtained by the micro-PIV.

Liquid phase: 0.5% SDS aqueous solution with 62% glycerol, $Q_g = 154$ μL/min; $Q_l = 200$ μL/min. (a) t ms, (b) $t + 133.33$ ms, (c) $t + 400$ ms, (d) $t + 1333.33$ ms, (e) $t + 533.33$ m, (f) $t + 1466.67$ ms. [Color figure can be viewed in the online issue, which is available at wileyonlinelibrary.com.]

Resistance of Small Bubbles in the Microchannel. The resistance of liquid filled microchannels containing small droplets can be calculated by the following equations

$$\Delta P = \Delta P_L + \Delta P_e \tag{12}$$

$$\Delta P_e = n_B \Delta P_B \tag{13}$$

$$\Delta P_B = \Delta P_L l_b / L \tag{14}$$

$$R = R_o + n_B R_B = R_o (1 + l_b/\lambda) \tag{15}$$

where l_b represents the additional resistance by each droplet in the channel with an unit of length. $R_B = R_o l_b / L$ is the excess hydrodynamic resistance due to each droplet.[21,33] λ ($\lambda = L/n_B$) is the distance between two successive droplets. For droplets smaller than the channel width, l_b/W is a dimensionless function of the viscosity ratio for the dispersed phase to the continuous one and of the geometrical factor l_B/W.[21] However, the exact expression for the additional resistance induced by small droplets and bubbles with respect to channels filled up by a pure liquid cannot be obtained at hand and should be improved in the future still. Therefore, for the small bubble case, the pressure drop along the channel is calculated using Eqs. 12 and 13, with ΔP_B is still calculated using Eq. 3 due to the dependence of additional pressure drop induced by small bubbles on the viscosity of the continuous phase.[31]

The predictions for the repartition of bubbles at the microfluidic T-junction are obtained using the aforementioned

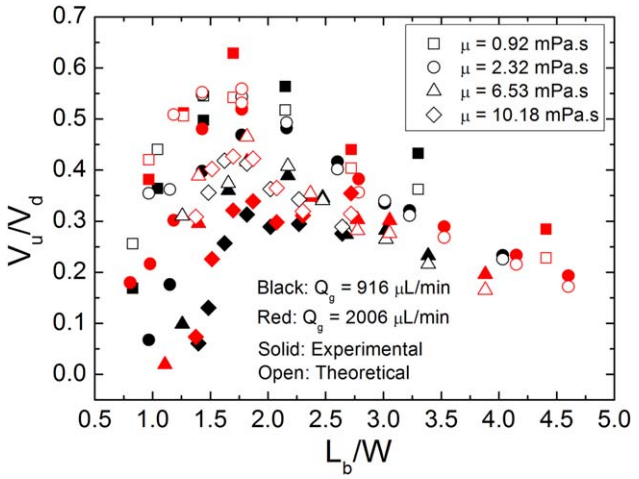

Figure 9. Comparison between the experimental data and the theoretical prediction for the splitting ratio of the bubble size at the T-junction.

[Color figure can be viewed in the online issue, which is available at wileyonlinelibrary.com.]

approaches, and the comparison between the theoretical values and the experimental data is illustrated in Figure 9. The calculated values compare satisfactorily with the experimental data for relatively long bubbles ($L_b/W \in [1.75,\ 4.0]$) under low liquid viscosities ($\mu \leq 6.53$mPa s). The slight discrepancy between the experimental data and the theoretical values may stem from the collision of bubbles at the second T-junction convergence as shown in Figure 10,[24,27,41] or from the simplifying assumptions used in constructing our model to use well-established pressure-flow relationship of Eq. 3. These collisions could dynamically modify the pressure equilibrium between two arms. The relatively large discrepancy between the experimental data and the theory for the high liquid viscosity might be due to the disjoining pressure in thin films of liquid in contact with the solid surface of the channel wall.[50] Therefore, it is also an urgent task to compensate the aforementioned predictions for the collision case[24,27] and the high viscosity case. Nevertheless, for the small bubbles case, the deviation exists as expected, but fortunately, the theoretical calculation can predict the increase of V_u/V_d with L_b/W. Furthermore, V_u/V_d can be obtained through the aforementioned theory for the resistance at the presence of bubbles in liquid filled channels to guide the tailoring of bubbles at a T-junction as $\frac{V_u}{V_u+V_d}=\frac{V_u/V_d}{V_u/V_d+1}$ and $\frac{V_d}{V_u+V_d}=\frac{1}{V_u/V_d+1}$.

Limitations and Suggestions. The pressure drop in the liquid filled microchannels containing slug bubbles includes three parts: the one along the slug bubble induced by the frictional loss in the liquid film and gutters between the bubble and the channel walls, the one induced by the Laplace pressure across the caps of the slug bubble, and the one in the liquid plug.[47] The pressure drop induced by the frictional loss in the liquid film and gutters between the bubble and the channel walls is often neglected in comparison with the other two kinds of pressure drops, both for bubbles in surfactant-free liquids and for the liquid phase with surfactants whose concentration is high enough [usually above its critical micelle concentration (CMC) value].[47,54–57] The former case is validated analytically using a matched-asymptotics method by Bretherton,[50] and the reason is because there is no dissipation in the middle stagnant film region for the cylindrical part of the bubble. The latter case is also validated theoretically by Stebe et al.[55] and experimentally by Fuerstman et al.[47] Stebe et al.[55] have shown that a surfactant-laden interface may mobilize when the bulk surfactant concentration is high enough, and the surfactant concentration is uniform along the interface, that is, the Marangoni forces are zero. Thus, the motion of a surfactant-laden bubble is the same as that of a surfactant-free bubble, with its surface tension is lower by a constant value everywhere on the interface. Fuerstman et al.[47] also confirmed experimentally that at high concentration of surfactant, molecules of the surfactant adsorb onto the interface rapidly and the surface of the bubble in the liquid flow cannot establish a gradient. With this rapid remobilization, the saturated interface is then the same as a bubble in surfactant-free liquid. However, for intermediate concentrations of surfactant in the liquid, the pressure decreases most rapidly across the body of the bubble owing to the gradient in the concentration of surfactant along the interface, giving rise to tangential surface tension tractions (Marangoni tractions) which can immobilize the interface. This would increase the pressure drop across the length of the bubble, because of the large shear stresses induced in the thin wetting film around the gas slug.[47,58] In this study, surfactant SDS is added to the continuous phase with a concentration of 0.5%, which is above twice of the CMC value of SDS (about 0.24%) in the continuous phase. It is assumed that the concentration of surfactant SDS is high enough to make the interface with uniform concentration of surfactant to behave like a bubble in surfactant-free liquid and the pressure drop along the cylindrical body of the bubble can be neglected to make sure that the pressure drop across bubbles can be obtained by using the Bretherton expression for low Ca[50] and Ratulowski and Chang expression for high Ca[53] as illustrated in Eq. 3.

The pressure drop of liquid filled microchannel containing slug bubbles is also influenced by the cross-section of the channel. Ratulowski and Chang established an empirical relationship between the pressure drop across a bubble and the capillary number in square cross-sectional microchannels

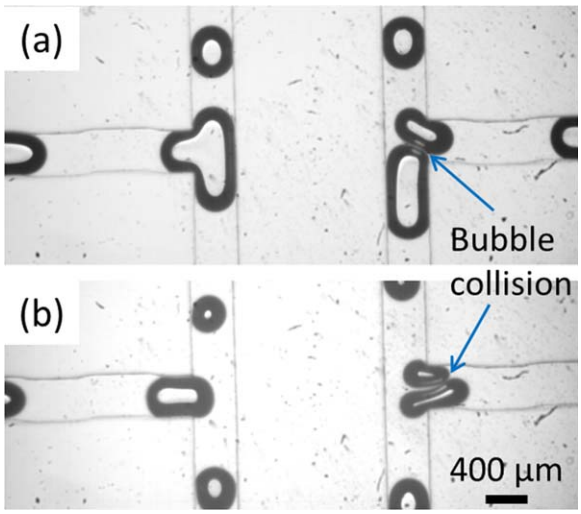

Figure 10. Bubble collision at the second T-junction convergence.

Liquid phase: 0.5% SDS aqueous solution. (a) Long bubble, $L_b/W = 3.30$; (b) Short bubble, $L_b/W = 1.70$. [Color figure can be viewed in the online issue, which is available at wileyonlinelibrary.com.]

as $\Delta P_B = 12.2 Ca^{0.55}$ for nonaxisymmetric cross-section of the bubble when $3\times10^{-3} < Ca < 0.1$.[53,59] This relationship is purely empirical and deviates from the theoretical one proposed by Bretherton for circular microchannels[50] and by Wong et al. for rectangular microchannels.[60] Wong et al.[60] extended Bretherton's analysis[50] to rectangular microchannels with the aid of numerical computation. Both groups found that ΔP_B scales as σ/r (r is the radius of the microchannel), and σ/r is proportional to $Ca^{2/3}$. However, the analysis by Wong et al.[60] do not provide an explicit function form for $\Delta P_B \sim \sigma Ca^{2/3}/r$. Although the expressions developed by Bretherton[50] and Ratulowski and Chang[53] are not strictly applicable to the square geometry, our results show the possibility of using previous laws to model the dynamics of slug bubbles in our channels. It is plausible to explain this by the fact that at high concentration of surfactant, the saturated interface behaves like a bubble in surfactant-free liquid, and liquid can no longer flow through the gutters between the bubble and the channel walls in the corners of the channel.[47] Thus, the pressure drop due to the viscous dissipation in the gutters can also be neglected in this case. Nevertheless, further studies on hydrodynamic feedback on bubble breakup in rectangular microchannels need to be improved experimentally and theoretically.[14,52,60–63]

The resistance induced by small bubbles or droplets to the liquid filled microchannels is far more than mature. The Panizza's group has developed a model to calculate the additional resistance induced by small droplets as shown in Eqs. 12–15.[21,33] However, an explicit expression is missing still for the relationship between the representitive resistance induced by small droplets and its size, as well as the viscosity ratio between the two phases. We attempted to obtain this relationship from the literature such as in Belloul et al.,[27] Glawdel et al.,[40] Coulliette and Pozrikidis,[64] but it can not help. For example, from Figure 5 in Belloul et al.,[27] we obtained $l_b/W = 5.51 l_B/W - 3.33$, with $0.6 < l_B/W < 1.2$, and the viscosity ratio between the dispersed phase and the continuous phase is about 1. Labrot et al.[65] found that the value of l_b remains approximately constant as long as the droplet viscosity is lower than the viscosity of the surrounding phase. However, Glawdel et al.[40] found that the value of l_b is sensitive to the viscosity ratio between the dispersed phase and the continuous phase. Furthermore, the representitive resistance induced by small bubbles can not be obtained from the literature, to the best of our knowledge. Therefore, the information on the additional resistance induced by small droplets and bubbles need to be improved experimentally and theoretically.

Conclusions

In summary, the breakup of bubbles at a microfluidic T-junction in an asymmetric loop is affected by the additional resistance in the presence of bubbles in downstream channels, which is dependent on the gas and liquid flow rates and the liquid viscosity. The additional resistance of a single bubble relies on its size: for the long bubble, the added resistance could be expressed by Bretherton equation[50] and Ratulowski and Chang equation,[53] which is related to the capillary number; whereas for the short bubble, the supplementary resistance could be expressed as a representative length, which is not well characterized and requires still further works. The hydrodynamic feedback of bubbles in downstream channels to the breakup dynamics of bubbles at the T-junction is owing to the variation of the local pressure, which is related to the pressure drop along the downstream channels. Our results suggest that the flow resistance due to the dispersed phase such as bubbles should be taken into account for the design of microfluidic distributors and parallel microreactors. Further studies on the bubble breakup at asymmetric T-junctions should be performed for various cross-sectional channels such as rectangular and circular for the arms of the T-junctions.

Acknowledgments

The financial supports for this project from the National Natural Science Foundation of China (21106093, 21276175), the Research Fund for the Doctoral Program of Higher Education (20110032120010), and the Program of Introducing Talents of Discipline to Universities (B06006) are gratefully acknowledged. T. Fu appreciates the aid from D. Funfschilling for the experiments, and the financial assistance from both the China Scholarship Council and the French Embassy in China.

Literature Cited

1. Perkel JM. Microfluidics-bringing new things to life science. *Science*. 2008;322:975–977.
2. Squires TM, Quake SR. Microfluidics: fluid physics at the nanoliter scale. *Rev Mod Phys*. 2005;77:977–1026.
3. Seemann R, Brinkmann M, Pfohl T, Herminghaus S. Droplet based microfluidics. *Rep Prog Phys*. 2012;75:016601.
4. Vladisavljević GT, Kobayashi I, Nakajima M. Production of uniform droplets using membrane, microchannel and microfluidic emulsification devices. *Microfluid Nanofluid*. 2012;13:151–178.
5. Zhao Y, Shum HC, Chen H, Adams LLA, Gu Z, Weitz DA. Microfluidic generation of multifunctional quantum dot barcode particles. *J Am Chem Soc*. 2011;133:8790–8793.
6. Fu T, Ma Y, Funfschilling D, Zhu C, Li HZ. Squeezing-to-dripping transition for bubble formation in a microfluidic T-junction. *Chem Eng Sci*. 2010;65:3739–3748.
7. Garstecki P, Fuerstman MJ, Stone HA, Whitesides GM. Formation of droplets and bubbles in a microfluidic T-junction—scaling and mechanism of break-up. *Lab Chip*. 2006;6:437–446.
8. Thorsen T, Roberts RW, Arnold FH, Quake SR. Dynamic pattern formation in a vesicle-generating microfluidic device. *Phys Rev Lett*. 2001;86:4163–4166.
9. Anna SL, Bontoux N, Stone HA. Formation of dispersions using "flow focusing" in microchannels. *Appl Phys Lett*. 2003;82:364–366.
10. Gañán-Calvo AM, Gordillo JM. Perfectly monodisperse microbubbling by capillary flow focusing. *Phys Rev Lett*. 2001;87:274501.
11. Fu T, Ma Y, Funfschilling D, Zhu C, Li HZ. Breakup dynamics of slender bubbles in non-Newtonian fluids in microfluidic flow-focusing devices. *AIChE J*. 2012;58:3560–3567.
12. deMello AJ. Control and detection of chemical reactions in microfluidic systems. *Nature*. 2006;442:394–402.
13. Valassis D, Dodde R, Esphuniyani B, Fowlkes J, Bull J. Microbubble transport through a bifurcating vessel network with pulsatile flow. *Biomed Microdevices*. 2012;14:131–143.
14. Baudoin M, Song Y, Manneville P, Baroud CN. Airway reopening through catastrophic events in a hierarchical network. *Proc Natl Acad Sci USA*. 2013;110:859–864.
15. Hashimoto M, Whitesides GM. Formation of bubbles in a multisection flow-focusing junction. *Small*. 2010;6:1051–1059.
16. Hashimoto M, Shevkoplyas SS, Zasońska B, Szymborski T, Garstecki P, Whitesides GM. Formation of bubbles and droplets in parallel, coupled flow-focusing geometries. *Small*. 2008;4:1795–1805.
17. Fuerstman MJ, Garstecki P, Whitesides GM. Coding/decoding and reversibility of droplet trains in microfluidic networks. *Science*. 2007;315:828–832.
18. Moritani T, Yamada M, Seki M. Generation of uniform-size droplets by multistep hydrodynamic droplet division in microfluidic circuits. *Microfluid Nanofluid*. 2011;11:601–610.
19. Link DR, Anna SL, Weitz DA, Stone HA. Geometrically mediated breakup of drops in microfluidic devices. *Phys Rev Lett*. 2004;92:054503.

20. Tan YC, Fisher JS, Lee AI, Cristini V, Lee AP. Design of microfluidic channel geometries for the control of droplet volume, chemical concentration, and sorting. *Lab Chip*. 2004;4:292–298.
21. Engl W, Roche M, Colin A, Panizza P, Ajdari A. Droplet traffic at a simple junction at low capillary numbers. *Phys Rev Lett*. 2005;95: 208304.
22. Hoang DA, Portela LM, Kleijn CR, Kreutzer MT, van Steijn V. Dynamics of droplet breakup in a T-junction. *J Fluid Mech*. 2013; 717:R4.
23. Schindler M, Ajdari A. Droplet traffic in microfluidic networks: a simple model for understanding and designing. *Phys Rev Lett*. 2008; 100:044501.
24. Belloul M, Engl W, Colin A, Panizza P, Ajdari A. Competition between local collisions and collective hydrodynamic feedback controls traffic flows in microfluidic networks. *Phys Rev Lett*. 2009;102: 194502.
25. Sessoms DA, Amon A, Courbin L, Panizza P. Complex dynamics of droplet traffic in a bifurcating microfluidic channel: periodicity, multistability, and selection rules. *Phys Rev Lett*. 2010;105: 154501.
26. Song Y, Manneville P, Baroud CN. Local interactions and the global organization of a two-phase flow in a branching tree. *Phys Rev Lett*. 2010;105:134501.
27. Belloul M, Courbin L, Panizza P. Droplet traffic regulated by collisions in microfluidic networks. *Soft Matter*. 2011;7:9453–9458.
28. Fu T, Ma Y, Funfschilling D, Li HZ. Dynamics of bubble breakup in a microfluidic T-junction divergence. *Chem Eng Sci*. 2011;66: 4184–4195.
29. Jullien MC, Ching MJTM, Cohen C, Menetrier L, Tabeling P. Droplet breakup in microfluidic T-junctions at small capillary numbers. *Phys Fluids*. 2009;21:072001.
30. Leshansky AM, Pismen LM. Breakup of drops in a microfluidic T junction. *Phys Fluids*. 2009;21:023303.
31. Jousse F, Farr R, Link DR, Fuerstman MJ, Garstecki P. Bifurcation of droplet flows within capillaries. *Phys Rev E*. 2006;74: 036311.
32. Engl W, Ohata K, Guillot P, Colin A, Panizza P. Selection of two-phase flow patterns at a simple junction in microfluidic devices. *Phys Rev Lett*. 2006;96:134505.
33. Sessoms DA, Belloul M, Engl W, Roche M, Courbin L, Panizza P. Droplet motion in microfluidic networks: hydrodynamic interactions and pressure-drop measurements. *Phys Rev E*. 2009;80: 016317.
34. Jeanneret R, Vest J-P, Bartolo D. Hamiltonian traffic dynamics in microfluidic-loop networks. *Phys Rev Lett*. 2012;108:034501.
35. Parthiban P, Khan SA. Filtering microfluidic bubble trains at a symmetric junction. *Lab Chip*. 2011;12:582–588.
36. Menetrier-Deremble L, Tabeling P. Droplet breakup in microfluidic junctions of arbitrary angles. *Phys Rev E*. 2006;74:035303.
37. Yamada M, Doi S, Maenaka H, Yasuda M, Seki M. Hydrodynamic control of droplet division in bifurcating microchannel and its application to particle synthesis. *J Colloid Interface Sci*. 2008;321:401–407.
38. Carlson A, Do-Quang M, Amberg G. Droplet dynamics in a bifurcating channel. *Int J Multiphase Flow*. 2010;36:397–405.
39. Bedram A, Moosavi A. Droplet breakup in an asymmetric microfluidic T junction. *Eur Phys J E*. 2011;34:78.
40. Glawdel T, Elbuken C, Ren C. Passive droplet trafficking at microfluidic junctions under geometric and flow asymmetries. *Lab Chip*. 2011;11:3774–3784.
41. Wu Y, Fu T, Zhu C, Lu Y, Ma Y, Li H. Asymmetrical breakup of bubbles at a microfluidic T-junction divergence: feedback effect of bubble collision. *Microfluid Nanofluid*. 2012;13:723–733.
42. Samie M, Salari A, Shafii MB. Breakup of microdroplets in asymmetric T junctions. *Phys Rev E*. 2013;87:053003.
43. Baroud CN, Tsikata S, Heil M. The propagation of low-viscosity fingers into fluid-filled branching networks. *J Fluid Mech*. 2006;546: 285–294.
44. Cristobal G, Benoit JP, Joanicot M, Ajdari A. Microfluidic bypass for efficient passive regulation of droplet traffic at a junction. *Appl Phys Lett*. 2006;89:034104.
45. van Steijn V, Kleijn CR, Kreutzer MT. Flows around confined bubbles and their importance in triggering pinch-off. *Phys Rev Lett*. 2009;103:214501.
46. Bruus H. *Theoretical Microfluidics*. New York: Oxford University Press, 2008.
47. Fuerstman MJ, Lai A, Thurlow ME, Shevkoplyas SS, Stone HA, Whitesides GM. The pressure drop along rectangular microchannels containing bubbles. *Lab Chip*. 2007;7:1479–1489.
48. Sullivan MT, Stone HA. The role of feedback in microfluidic flow-focusing devices. *Philos Trans R Soc Ser A*. 2008;366:2131–2143.
49. Fu T, Funfschilling D, Ma Y, Li HZ. Scaling the formation of slug bubbles in microfluidic flow-focusing devices. *Microfluid Nanofluid*. 2010;8:467–475.
50. Bretherton FP. The motion of long bubbles in tubes. *J Fluid Mech*. 1961;10:166–188.
51. Leshansky AM, Afkhami S, Jullien MC, Tabeling P. Obstructed breakup of slender drops in a microfluidic T junction. *Phys Rev Lett*. 2012;108:264502.
52. Ody CP, Baroud CN, de Langre E. Transport of wetting liquid plugs in bifurcating microfluidic channels. *J Colloid Interface Sci*. 2007; 308:231–238.
53. Ratulowski J, Chang H-C. Transport of gas bubbles in capillaries. *Phys Fluids A*. 1989;1:1642–1655.
54. Ratulowski J, Chang H-C. Marangoni effects of trace impurities on the motion of long gas bubbles in capillaries. *J Fluid Mech*. 1990; 210:303–328.
55. Stebe KJ, Lin S-Y, Maldarelli C. Remobilizing surfactant retarded fluid particle interfaces. I. Stress-free conditions at the interfaces of micellar solutions of surfactants with fast sorption kinetics. *Phys Fluids A*. 1991;3:3–20.
56. Abadie T, Aubin J, Legendre D, Xuereb C. Hydrodynamics of gas–liquid Taylor flow in rectangular microchannels. *Microfluid Nanofluid*. 2012;12:355–369.
57. Yu Z, Hemminger O, Fan L-S. Experiment and lattice Boltzmann simulation of two-phase gas–liquid flows in microchannels. *Chem Eng Sci*. 2007;62:7172–7183.
58. Chen J-D. Measuring the film thickness surrounding a bubble inside a capillary. *J Colloid Interface Sci*. 1986;109:341–349.
59. Kolb WB, Cerro RL. The motion of long bubbles in tubes of square cross section. *Phys Fluids A*. 1993;5:1549–1557.
60. Wong H, Radke CJ, Morris S. Motion of long bubbles in polygonal capillaries. Part 2. Drag, fluid pressure and fluid flow. *J Fluid Mech*. 1995;292:95–110.
61. Hazel AL, Heil M. The steady propagation of a semi-infinite bubble into a tube of elliptical or rectangular cross-section. *J Fluid Mech*. 2002;470:91–114.
62. de Lózar A, Hazel AL, Juel A. Scaling properties of coating flows in rectangular channels. *Phys Rev Lett*. 2007;99:234501.
63. Smith BJ, Gaver DP. Agent-based simulations of complex droplet pattern formation in a two-branch microfluidic network. *Lab Chip*. 2010;10:303–312.
64. Coulliette C, Pozrikidis C. Motion of an array of drops through a cylindrical tube. *J Fluid Mech*. 1998;358:1–28.
65. Labrot V, Schindler M, Guillot P, Colin A, Joanicot M. Extracting the hydrodynamic resistance of droplets from their behavior in microchannel networks. *Biomicrofluidics*. 2009;3:12804.

Manuscript received July 6, 2013, revision received Oct. 21, 2013, and final revision received Jan. 16, 2014.